Scientia Iranica F (2014) 21(3), 1129–1142

Sharif University of Technology
Scientia Iranica
Transactions F: Nanotechnology
www.scientiairanica.com

Effect of position of a square-shaped heat source on buoyancy-driven heat transfer in a square cavity filled with nanofluid

A. Arefmanesh[a], M. Mahmoodi[a,b,*] and M. Nikfar[c]

a. *Department of Mechanical Engineering, University of Kashan, Ghotb-e-Ravandi Boulevard, Kashan, Iran.*
b. *Department of Mechanical Engineering, Amirkabir University of Technology, 424 Hafez Ave, Tehran, Iran.*
c. *Department of Mechanical Engineering, K.N. Toosi University of Technology, 470 Mirdamad Ave. West, 19697, Tehran, Iran.*

Received 18 December 2012; received in revised form 22 June 2013; accepted 30 December 2013

KEYWORDS
Natural convection;
Nanofluid;
Heat source;
Square cavity;
Finite volume method.

Abstract. Buoyancy-driven heat transfer, due to a square-shaped heater placed inside a square cavity filled with TiO_2-water nanofluid, is investigated numerically. The heater is maintained at a constant temperature, T_h, while the cavity walls are kept at a lower constant temperature, T_c. The governing equations are solved using the finite volume method and the SIMPLER algorithm. The simulations are performed for six different positions of the heat source inside the cavity, a range of Rayleigh numbers from 10^3 to 10^6, and different volume fractions of the nanoparticles. The ratio of the height (width) of the heat source to that of the cavity is taken as 0.2. The results shows that the fluid flow and heat transfer characteristics inside the cavity strongly depend on the location of the heat source. For Ra $= 10^3$, i.e. a conduction-dominated heat transfer regime, maximum heat transfer rate is achieved by placing the heat source close to the corners of the cavity, while, for Ra $= 10^6$, positioning the heat source near the middle of the cavity's bottom wall yields the maximum average Nusselt number. Moreover, it is observed that the average Nusselt number is generally an increasing function of the volume fraction of the nanoparticles.

1. Introduction

Natural convection fluid flow and heat transfer inside enclosures are encountered in a number of industrial applications, such as solar collectors, heat exchangers, home ventilation, and electronic cooling devices. The low thermal conductivity of conventional fluids such as water and oil is a preeminent disadvantage in heat exchanging apparatus. Recently, nanofluids, which have relatively higher thermal conductivity compared to that of pure fluids, have been considered to enhance the rate of heat transfer in such devices.

*. *Corresponding author. Tel.: +98 9126514920*
E-mail addresses: arefmanesh@kashanu.ac.ir (A. Arefmanesh); mahmoodi.m@hotmail.com (M. Mahmoodi); nikfar.mehdi@gmail.com (M. Nikfar)

Khanafer et al. [1] are among the first investigators to have studied natural convection heat transfer in nanofluid-filled enclosures numerically. They observed that for the considered range of Grashof number, the Nusselt number increased with an increase in the volume fraction of the nanoparticles. Abu-Nada et al. [2] employed the finite volume method to investigate the buoyancy-driven heat transfer in a space between two differentially-heated concentric cylinders filled with nanofluids. Based on their observations, for high Rayleigh numbers, the heat transfer was significantly enhanced for nanoparticles with high thermal conductivity, while, for intermediate values of Rayleigh number, using nanoparticles with low thermal conductivity resulted in reductions in heat transfer rate. In another numerical study, Santra et al. [3] considered the buoyancy-driven fluid flow and heat transfer of Cu-

water nanofluid in a differentially-heated square cavity. They observed that the heat transfer rate decreased with increasing the volume fraction of the nanoparticles for Rayleigh numbers between 10^4 and 10^7. Oztop and Abu-nada [4] used the finite volume method to study the natural convection heat transfer in a Cu-water nanofluid-filled rectangular cavity with a cold vertical wall, an imbedded heater counterpart wall, and insulated horizontal walls. Their results showed that the average Nusselt number increased with increasing the volume fraction of the nanoparticles for Rayleigh numbers between 10^3 and 10^5. In another numerical work, Abu-nada and Oztop [5] used the finite volume method to study natural convection heat transfer in an inclined square cavity filled with Cu-water nanofluid. Their results indicated that addition of nanoparticles to the base fluid resulted in significant heat transfer enhancement. Aminossadati and Ghasemi [6] investigated the free convection of different water-based nanofluids in a square cavity having a constant flux heater on its horizontal bottom wall, numerically. The remaining cavity walls were kept at a relatively lower temperature. They observed that adding nanoparticles to water improved the heat transfer performance. Ghasemi and Aminossadati [7] studied periodic natural convection of nanofluid in a square cavity with insulated top and bottom walls, a cold right vertical wall, and an oscillating flux heat source on its left vertical wall. They observed that adding nanoparticles to the base fluid enhanced heat transfer, especially at low Rayleigh numbers. Oztop et al. [8] conducted a numerical study on free convection in a nanofluid-filled inclined square enclosure, subjected to heating and cooling by sinusoidal temperature profiles on one of its sides. They reported enhancements of heat transfer rate for the entire range of considered Rayleigh numbers. In another study, Sheikhzadeh et al. [9] investigated the natural convection of TiO_2-water nanofluid in rectangular cavities, with differentially-heated left and top walls and insulated remaining walls. Their results showed that by increasing the volume fraction of the nanoparticles, the average Nusselt number of the hot wall increased for shallow cavities, while a contrary trend was observed for tall ones. Analytical and numerical results on the free convection of a nanofluid in a shallow cavity heated from below and cooled from the ceiling were reported by Alloui et al. [10]. They observed that the enhancement of heat transfer due to the presence of nanoparticles depended on the value of the Rayleigh number. A numerical study on natural convection of CuO-water nanofluid in a cavity with two pairs of heat source-sink on its bottom wall was conducted by Aminossadati and Ghasemi [11]. Their results showed that regardless of the position of the pairs of source-sink, the heat transfer rate increased with increasing the Rayleigh number and the volume fraction of the nanoparticles. In another numerical study, Nasrin and Parvin [12] used the finite volume method to investigate the free convection heat transfer in a trapezoidal cavity with differentially heated side walls filled with Cu-water nanofluid. They observed that Cu nanoparticles with the lowest aspect ratio are established to be most effective in enhancing the performance of heat transfer rate. Nikfar and Mahmoodi [13] investigated the free convection heat transfer of a nanofluid in a square cavity with wavy side walls using the meshless local Petrov-Galerkin method.

As far as very recent studies on the natural convection inside nanofluid-filled enclosures with a hot block or rib on the wall are concerned, Mahmoudi et al. [14] conducted a numerical study on the natural convection cooling of a heat source horizontally attached to the left vertical wall of a cavity filled with copper-water nanofluid. They observed that the average Nusselt number increased with Rayleigh number and volume fraction of the nanoparticles, while it decreased with an increase in length of the heater. In another work, Mahmoudi et al. [15] studied the natural convection of copper-water nanofluid in an open cavity with two vertically mounted heaters on the horizontal walls. Their results indicated that the flow and temperature fields were strongly dependent on the Rayleigh number and the position of the heat sources. Effects of nanoparticles on enhancement of heat transfer in a U-shaped cavity were studied by Cho et al. [16]. Mahmoodi [17] and Mahmoodi and Hashemi [18], in two consecutive papers, conducted finite volume numerical studies of the natural convection heat transfer in L- and C-shaped cavities containing nanofluids, respectively. They concluded that the effect of nanoparticles on the heat transfer enhancement for narrow enclosures was more than that for wide enclosures. Dehnavi and Rezvani [19] considered a Γ-shaped cavity and studied natural convection of Al_2O_3-water nanofluid inside it.

There are some papers on the natural convection of nanofluids in enclosures with inside heaters of different shape. In a numerical study, Mahmoodi [20] investigated the effect of nanofluid on heat transfer in a square cavity with a vertical or horizontal inside thin heater. Entropy generation, due to natural convection around a horizontal heat source in a square cavity containing nanofluid, was studied by Shahi et al. [21]. Some observations about natural convection of nanofluids in a square cavity with differentially heated side walls and insulated horizontal walls can be found in the works of Sheikhzadeh et al. [22], Mahmoodi and Sebdani [23] and Aminossadati and Ghasemi [24]. Arefmanesh et al. [25] studied the buoyancy-driven heat transfer in two-square duct annuli filled with TiO_2-water nanofluid. They conducted a parametric study involving the effects of Rayleigh number, annulus

aspect ratio, and the volume fraction of nanoparticles on fluid flow and heat transfer. Their results showed heat transfer enhancement in the presence of the nanoparticles. The results obtained by Matin and Pop [26] about natural convection of nanofluids in eccentric annuluses stated that the position of the inner cylinder had a major effect on the rate of heat transfer. The above detailed literature survey reveals that, although many studies have been conducted on natural convection fluid flow and heat transfer in nanofluid-filled enclosures with different boundary conditions, no study exists on the effect of the position of a square-shaped heat source in a nanofluid-filled cavity on the buoyancy-driven heat transfer inside the cavity. According to the findings of Matin and Pop [26], the position of a heater in a cavity is an important parameter in the natural convection heat transfer process. The present study, therefore, concentrates only on this.

2. Problem formulation

A schematic diagram of the system composed of a square-shaped heat source inside the square cavity and the coordinates are depicted in Figure 1. Each side of the heat source and, also, each side of the cavity are denoted by h and H, respectively. The lengths of the heat square and the cavity perpendicular to the plane of the figure are long enough for the problem to be considered two-dimensional. The heat source and the cavity are maintained at differentially-different constant temperatures of T_h and T_c, respectively, with $T_h > T_c$. A special coordinate system (s) along the walls of the cavity is adopted with its origin at $x = 0$ and $y = 0$, as identified by the dashed line in Figure 1. A dimensionless form of the special coordinate system is defined as $S = s/H$. The cavity is filled with

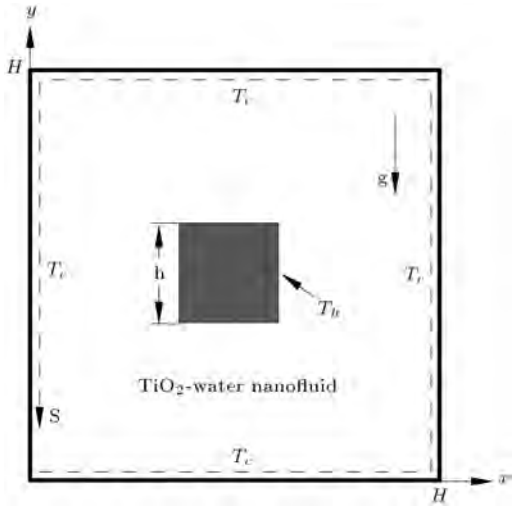

Figure 1. Natural convection due to a square-shaped heat source inside a cold square cavity.

Table 1. Thermophysical properties of the base fluid and nanoparticles [4].

Physical properties	Base fluid (water)	Nanoparticles (TiO_2)
C_p (J/kg-K)	4179	686.2
ρ (kg/m^3)	997.1	4250
k (W/m-K)	0.613	8.9538
$\beta \times 10^5$ (K^{-1})	21	0.9
μ (kg/m-s)	0.001003	—

a nanofluid composed of water and TiO_2 spherical nanoparticles. The nanofluid is assumed to be incompressible, and the nanoparticles are presumed to be in thermal equilibrium with the base fluid. Moreover, there is no slip between the nanoparticles and the water. The thermophysical properties of the base fluid and the nanoparticles are presented in Table 1. The nanofluid properties are considered to be constant, with the exception of its density in the buoyancy term of the momentum equation, which varies according to the Boussinesq approximation [27].

The equations for conservation of mass, momentum, and energy for the two-dimensional steady laminar flow of the nanofluid, incorporating natural convection via the Boussinesq approximation, are given by:

$$\frac{\partial u}{\partial x} + \frac{\partial v}{\partial y} = 0, \tag{1}$$

$$u\frac{\partial u}{\partial x} + v\frac{\partial u}{\partial y} = -\frac{1}{\rho_{\rm nf}}\frac{\partial p}{\partial x} + \frac{\mu_{\rm nf}}{\rho_{\rm nf}}\left(\frac{\partial^2 u}{\partial x^2} + \frac{\partial^2 u}{\partial y^2}\right), \tag{2}$$

$$u\frac{\partial v}{\partial x} + v\frac{\partial v}{\partial y} = -\frac{1}{\rho_{\rm nf}}\frac{\partial p}{\partial y} + \frac{\mu_{\rm nf}}{\rho_{\rm nf}}\left(\frac{\partial^2 v}{\partial x^2} + \frac{\partial^2 v}{\partial y^2}\right) + \frac{(\rho\beta)_{\rm nf} g(T - T_c)}{\rho_{\rm nf}}, \tag{3}$$

and:

$$u\frac{\partial T}{\partial x} + v\frac{\partial T}{\partial y} = \alpha_{\rm nf}\left(\frac{\partial^2 T}{\partial x^2} + \frac{\partial^2 T}{\partial y^2}\right). \tag{4}$$

A dimensionless form of the governing equations can be obtained via introducing the following dimensionless variables:

$$X = \frac{x}{H}, \quad Y = \frac{y}{H}, \quad U = \frac{uH}{\alpha_f},$$

$$V = \frac{vH}{\alpha_f}, \quad P = \frac{pH^2}{\rho_{\rm nf}\alpha_f^2}, \quad \text{and} \quad \theta = \frac{T - T_c}{T_h - T_c}. \tag{5}$$

Substituting the above non-dimensional variables into the continuity, momentum, and energy equations re-

sults in the following dimensionless form of the governing equations:

$$\frac{\partial U}{\partial X}+\frac{\partial V}{\partial Y}=0, \tag{6}$$

$$U\frac{\partial U}{\partial X}+V\frac{\partial U}{\partial Y}=-\frac{\partial P}{\partial X}+\frac{\mu_{\rm nf}}{\rho_{\rm nf}\alpha_f}(\frac{\partial^2 U}{\partial X^2}+\frac{\partial^2 U}{\partial Y^2}), \tag{7}$$

$$U\frac{\partial V}{\partial X}+V\frac{\partial V}{\partial Y}=-\frac{\partial P}{\partial Y}+\frac{\mu_{\rm nf}}{\rho_{\rm nf}\alpha_f}(\frac{\partial^2 V}{\partial X^2}+\frac{\partial^2 V}{\partial Y^2})+\frac{(\rho\beta)_{\rm nf}}{\rho_{\rm nf}\beta_f}{\rm RaPr}\theta, \tag{8}$$

and:

$$U\frac{\partial \theta}{\partial X}+V\frac{\partial \theta}{\partial Y}=\frac{\alpha_{\rm nf}}{\alpha_f}(\frac{\partial^2 \theta}{\partial X^2}+\frac{\partial^2 \theta}{\partial Y^2}), \tag{9}$$

where Rayleigh number, Ra, and Prandtl number, Pr, are defined as follows:

$${\rm Ra}=\frac{g\beta_f(T_h-T_c)H^3}{\alpha_f v_f},\quad \text{and}\quad {\rm Pr}=\frac{v_f}{\alpha_f}. \tag{10}$$

The boundary conditions for Eqs. (6)-(9) are:

$$U=V=0,\quad \theta=1\quad \text{on the heat source,}$$

and:

$$U=V=0,\quad \theta=0\quad \text{on the walls of the cavity.} \tag{11}$$

2.1. Thermophysical properties of the nanofluid

The effective viscosity, $\mu_{\rm nf}$, of the nanofluid can be estimated by the following empirical correlation proposed by Corcione [28]:

$$\frac{\mu_{\rm nf}}{\mu_f}=\frac{1}{1-34.87(d_s/d_f)^{-0.3}\varphi^{1.03}}, \tag{12}$$

where d_f is the equivalent diameter of base fluid molecules and given by:

$$d_f=0.1\left(\frac{6M}{N\pi\rho_{f0}}\right)^{1/3}, \tag{13}$$

in which M is the molecular weight of the base fluid, N is the Avogadro number, and ρ_{f0} is the mass density of the base fluid calculated at temperature $T_0=293$ K. The viscosity of the base fluid (water) varies with temperature, according to the following equation:

$$\mu_{\rm H_2O}=\Big(1.2723\times T_{rc}^5-8.736\times T_{rc}^4+33.708\times T_{rc}^3-246.6\times T_{rc}^2+518.78\times T_{rc}+1153.9\Big)\times 10^{-6}, \tag{14}$$

where $T_{rc}=\log(T-273)$. Also, the thermal conductivity, $k_{\rm nf}$, of the nanofluid can be obtained from the empirical correlation proposed by Corcione [28]:

$$\frac{k_{\rm nf}}{k_f}=1+4.4\varphi^{0.66}\left(\frac{T}{T_{\rm fr}}\right)^{10}\left(\frac{k_s}{k_f}\right)^{0.03}{\rm Pr}^{0.66}{\rm Re}^{0.4}, \tag{15}$$

where T is the nanofluid temperature, $T_{\rm fr}$ is the freezing point of the base liquid, k_s is the nanoparticle thermal conductivity, Pr is the Prandtl number of the base liquid, and Re is the nanoparticle Reynolds number, defined as:

$${\rm Re}=\frac{2\rho_f k_b T}{\pi\mu_f^2 d_s}, \tag{16}$$

where symbol k_b is the Boltzmann constant ($k_b=1.3807\times 10^{-23}$ J / K).

The density, $\rho_{\rm nf}$, heat capacity, $(\rho c_p)_{\rm nf}$, and thermal expansion coefficient, $(\rho\beta)_{\rm nf}$, of the nanofluid are obtained from the following respective relations [4]:

$$\rho_{\rm nf}=(1-\varphi)\rho_f+\varphi\rho_p, \tag{17}$$

$$(\rho c_p)_{\rm nf}=(1-\varphi)(\rho c_p)_f+\varphi(\rho c_p)_p, \tag{18}$$

and:

$$(\rho\beta)_{\rm nf}=(1-\varphi)(\rho\beta)_f+\varphi(\rho\beta)_p. \tag{19}$$

The thermal diffusivity of the nanofluid, $\alpha_{\rm nf}$, is evaluated from the following relation:

$$\alpha_{\rm nf}=\frac{k_{\rm nf}}{(\rho c_p)_{\rm nf}}. \tag{20}$$

The Nusselt number based on the height (width) of the cavity is evaluated from the following relation:

$${\rm Nu}=\frac{h_{\rm nf}H}{k_f}. \tag{21}$$

The heat transfer coefficient for the nanofluid, $h_{\rm nf}$, is obtained from the following equation:

$$h_{\rm nf}=\frac{q}{T_h-T_c}, \tag{22}$$

where the wall heat flux per unit area, q, can be written as:

$$q=-k_{\rm nf}\frac{T_h-T_c}{H}\frac{\partial\theta}{\partial n}|_{\rm wall}. \tag{23}$$

Substituting Eqs. (22) and (23) into Eq. (21) yields the following relation for the Nusselt number along the walls of the cavity:

$${\rm Nu}=-(\frac{k_{\rm nf}}{k_f})\frac{\partial\theta}{\partial n}|_{\rm wall}. \tag{24}$$

3. Computational details

The solution of the governing equations leads to a complete understanding of the velocity and temperature fields for natural convection due to the square-shaped heat source inside the cavity. Consequently, the effects of the position and the temperature of the heat square on the flow and thermal fields can be evaluated. The steady-state mass, momentum, and energy governing equations, written in terms of the primitive variables, are discretized using the finite volume method and the SIMPLER algorithm [29]. To implement the numerical method, a regular, two-dimensional, finite difference grid is generated in the computational domain. Subsequently, a square-shaped control volume is generated around each of the grid points. The governing equations are then integrated over each control volume. In the next step, the derivatives of the dependent variables on the faces of the control volume in the resulting equations are replaced by finite difference approximations written in terms of the nodal values of the dependent variables. A second-order central difference scheme is used for the diffusion terms, while a hybrid scheme, a combination of upwind and central difference schemes, is employed for the convective terms [28]. Carrying out the same procedure for all of the control volumes in the computational domain yields a system of algebraic equations with the nodal values of the dependent variables as unknowns. The set of discretized equations are then solved iteratively, yielding the values of velocity, pressure, and temperature at the grid points. An under-relaxation scheme is employed to obtain the converged solution.

3.1. Benchmarking of the code

In order to validate the numerical procedure, the buoyancy-driven fluid flow and heat transfer in a partially-heated square cavity filled with Cu-water nanofluid is simulated numerically using the proposed code, and the results are compared with the existing results in the literature.

Figure 2 shows the domain and the boundary conditions for the buoyancy-driven heat transfer in a partially-heated square cavity filled with Cu-water nanofluid. A heat source with a constant temperature, T_h, whose length is equal to half of the cavity's height, is placed symmetrically along the left wall of the cavity. The right side wall of the cavity is maintained at a constant temperature, T_c, with $T_c < T_h$. The top and bottom walls, as well as the remaining portion of the left side wall, are kept insulated. The simulations are performed for different volume fractions of the nanoparticles, including $\varphi = 0$ (pure water), and for $\mathrm{Ra} = 10^3$, 10^4, and 10^5. An 80×80 uniform grid is employed for the numerical simulations. Table 2 shows comparisons between the average Nusselt number of the heat source obtained by the present code with the results of Oztop and Abu-Nada [4] for different volume fractions of the nanoparticles at different Rayleigh numbers. As observed from this table, very good agreement exists between the two results for the considered ranges of Rayleigh number and volume fraction of the nanoparticles.

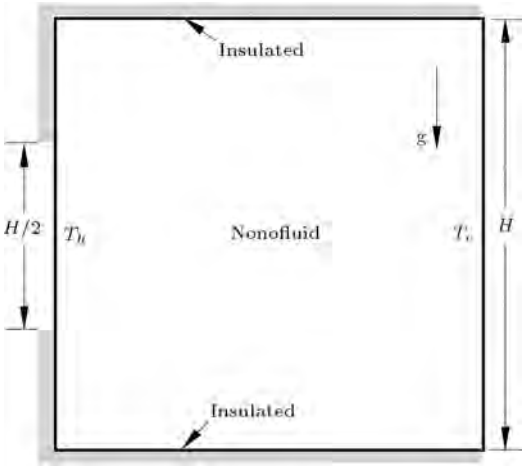

Figure 2. Natural convection in a square cavity with a partially-heated wall filled with Cu-water nanofluid.

Table 2. Average Nusselt number of the heat source for the partially-heated square cavity filled with Cu-water nanofluid; comparisons with Oztop and Abu-Nada [4].

Ra	φ	Present study	Oztop and Abu-Nada [4]
10^3	0.00	1.045	1.004
	0.05	1.131	1.122
	0.10	1.255	1.251
	0.15	1.450	1.423
	0.20	1.665	1.627
10^4	0.00	2.001	2.010
	0.05	2.098	2.122
	0.10	2.155	2.203
	0.15	2.276	2.283
	0.20	2.355	2.363
10^5	0.00	3.973	3.983
	0.05	4.266	4.271
	0.10	4.352	4.440
	0.15	4.651	4.662
	0.20	4.865	4.875

3.2. Grid independence study

In order to determine a proper grid for the numerical simulations, a grid independence study is conducted for the buoyancy-driven heat transfer due to the square-shaped heat source placed at the center of the square cavity filled with TiO_2-water nanofluid (Figure 1). The

Table 3. Average Nusselt number of the square cavity for different uniform grids, $h/H = 0.2$, $\varphi = 0.015$ and $\mathrm{Ra} = 10^6$.

Number of nodes	40×40	60×60	80×80	100×100	120×120
$\mathbf{Nu_{avg}}$	2.6516	3.1074	3.4112	3.4127	3.4130

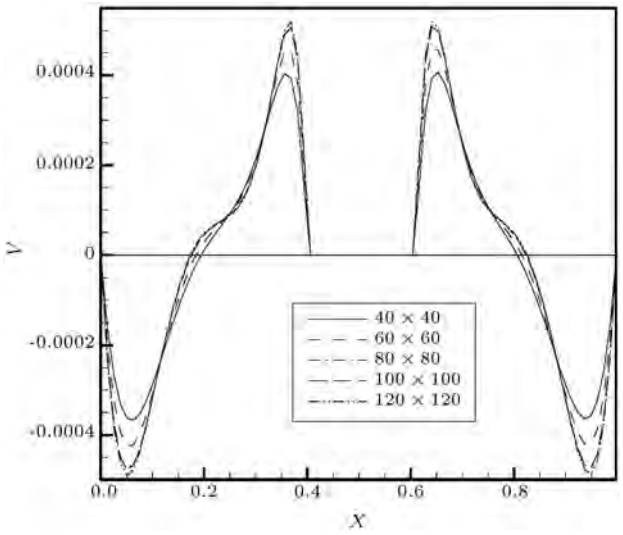

Figure 3. Vertical velocity component along the horizontal centerline of the cavity ($y = H/2$) for different uniform grids, $h/H = 0.2$, $\varphi = 0.015$, and $\mathrm{Ra} = 10^6$.

simulations are performed for $h/H = 0.2$, $\mathrm{Ra} = 10^6$, and $\varphi = 0.015$. Five different uniform grids, namely, 40×40, 60×60, 80×80, 100×100 and 120×120, are employed for the numerical calculations.

Figure 3 shows the vertical velocity component along the horizontal centerline of the cavity ($y = H/2$, Figure 1) for these grids. The results for the average Nusselt number of the cavity for the above grids are also presented in Table 3. It is observed from Figure 3 and Table 3 that an 80×80 uniform grid is sufficiently fine to capture the details of the velocity and temperature variations in the boundary layers adjacent to the walls. Therefore, based on these results, an 80×80 uniform grid is employed to perform all subsequent numerical calculations. Moreover, in the numerical calculations, the convergence criterion for the temperature, pressure, and velocity is taken to be:

$$\mathrm{Error} = \frac{\sum_{j=1}^{m}\sum_{i=1}^{n}|\xi^{t+1} - \xi^{t}|}{\sum_{j=1}^{m}\sum_{i=1}^{n}|\xi^{t+1}|} \leq 10^{-7}, \tag{25}$$

where m and n are the number of grid points in the x and y directions, respectively, ξ is any of the computed field variables, and t is the iteration number.

4. Results and discussion

In order to understand the flow and heat transfer characteristics of the considered problem, six different

Table 4. Coordinates of the center of the heat source for the six considered cases.

Case number	***x*-coordinate**	***y*-coordinate**
I	$H/2$	$H/2$
II	$H/2$	$H/4$
III	$H/4$	$H/4$
IV	$H/4$	$H/2$
V	$H/4$	$3H/4$
VI	$H/2$	$3H/4$

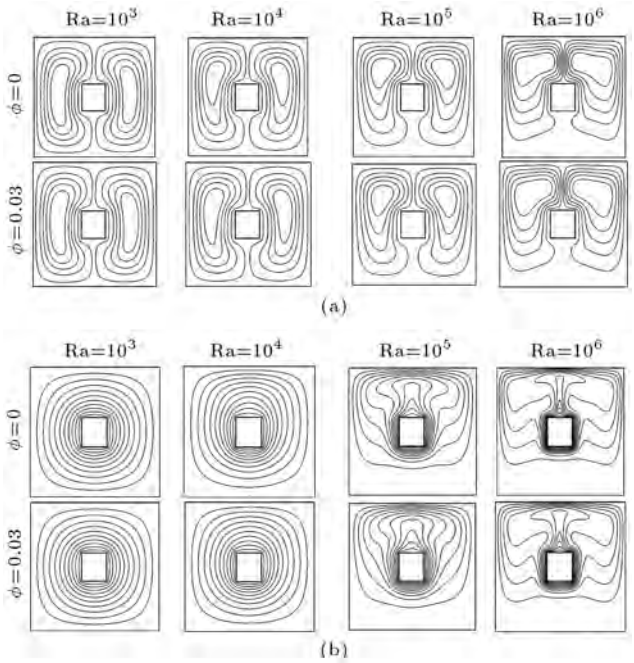

Figure 4. Streamlines and isotherms in the cavity filled with TiO_2-water for case I: (a) Streamlines; and (b) isotherms.

cases, cases I through VI, as far as the position of the heat source inside the cavity is concerned, are considered. The coordinates of the center of the heat source for the six considered cases are given in Table 4. In all the following numerical results, the ratio of the size of the heat source to that of the cavity, h/H, is taken as 0.2, and the cavity is filled with the TiO_2-water nanofluid. The simulations are performed for a range of Rayleigh numbers from 10^3 to 10^6, and for three volume fractions of the nanoparticles, namely, 0 (pure water), 0.015 and 0.03.

Figure 4(a) and (b) show the streamlines and the isotherms inside the cavity for case I, respectively. The results in these figures are presented for the volume fraction of the nanoparticles, $\varphi = 0$ and 0.03, and

for different Rayleigh numbers. The fluid is heated by the left and right side walls of the heat source and expands as it moves upwards. Subsequently, along the downflowing branch of the cycle, the fluid is cooled by the cold walls of the cavity, and compressed as it reaches the depth of the cavity. Hence, as Figure 4(a) shows, two counter-rotating eddies, clockwise and a counterclockwise, develop in the right and left halves of the space between the heat source and the cavity. For low Rayleigh numbers, i.e. conduction-dominated fluid flow and heat transfer, these eddies, symmetrically-located, with respect to the centerlines of the cavity (Figure 4(a) for Ra $= 10^3$), are quite weak. With increasing Rayleigh number, the two main eddies strengthen as their centers shift towards the top wall of the cavity (Figure 4(a) for Ra $\geq 10^4$); however, they constantly remain symmetric with respect to the vertical centerline of the cavity. For high enough Rayleigh numbers (Ra $= 10^6$ in Figure 4(a)), the hot bottom wall of the heat source resists the natural convection in the bottom of the cavity, resulting in a relatively stagnant region.

The corresponding isotherms inside the cavity for case I are shown in Figure 4(b). For low Rayleigh numbers (Figure 4(b) for Ra $= 10^3$), the isotherms are almost evenly-distributed in the space between the heat source and the walls of the cavity. Increasing the Rayleigh number gives rise to the formation of thermal boundary layers around the heat source, as well as close to the top and upper portions of the side walls of the cavity, bringing about greater heat transfer rates in these regions (Figure 4(b) for Ra $\geq 10^5$). Meanwhile, the isotherms, similar to the streamlines, always remain symmetric with respect to the vertical centerline of the cavity. Moreover, for high Rayleigh numbers, the core of the two main eddies is relatively stagnant and thermally stratified, and the stagnant region under the heat source is nearly isothermal, with a minimum heat transfer rate (Figure 4(b) for Ra $\geq 10^5$).

The streamlines and the isotherms inside the cavity for case II are shown in Figure 5(a) and (b), respectively. As observed from Figure 5(a), two main counter-rotating eddies, which are symmetric only with respect to the vertical centerline of the cavity, form inside the cavity. The center of these eddies moves upwards as the natural convection strengthens with increasing the Rayleigh number. As the heat source is moved towards the bottom of the cavity, the stagnant region under its bottom wall shrinks (Figure 5(a) for Ra $\geq 10^5$), improving the heat transfer rate there. As far as the isotherms are concerned, for low Rayleigh numbers, they are densely distributed in the narrow space between the bottom of the heat source and the cavity's bottom wall, and thinly scattered above the heat source, resulting in high and low temperature gradients under and above the heat source, respectively

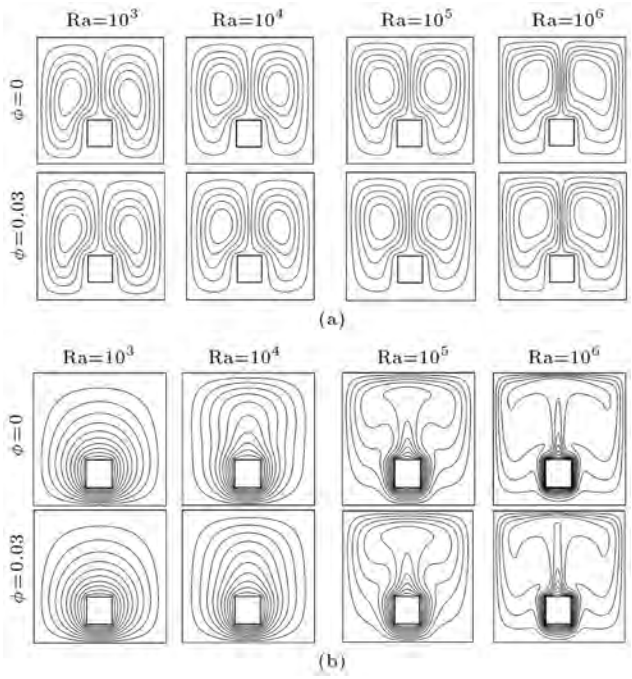

Figure 5. Streamlines and isotherms in the cavity filled with TiO_2-water for case II: (a) Streamlines; and (b) isotherms.

(Figure 5(b) for Ra $\leq 10^4$). For high Rayleigh numbers, thermal boundary layers form around the heat source and close to the top wall of the cavity, indicating high heat transfer rates in these regions. Moreover, large regions close to the center of the main eddies remain nearly isothermal (Figure 5(b) for Ra $= 10^6$).

Figure 6(a) and (b) show the streamlines and the isotherms inside the cavity for case III. By moving the heat source towards the left bottom corner of the cavity, a main clockwise vortex develops due to the natural convection in the relatively large space to the right of the heat source. Another smaller counterclockwise vortex forms in the left portion of the cavity above the heat source (Figure 6(a)). With increasing the Rayleigh number, the natural convection above the heat source intensifies, and the counterclockwise eddy enlarges. Meanwhile, the narrow regions to the left and under the bottom of the heat source always remain relatively stagnant (Figure 6(a)). As far as the isotherms are concerned, the above-mentioned narrow regions are dominated by heat conduction, even for high Rayleigh numbers (Figure 6(b)). Moreover, as the Rayleigh number increases, thermal boundary layers form close to the top and left walls of the cavity with high temperature gradient toward the left and close to the top of the cavity's top and left walls, respectively, giving rise to high heat transfer rates in these regions. (Figure 6(b) for Ra $= 10^6$).

The streamlines and the isotherms inside the cavity for case IV are presented in Figure 7(a) and

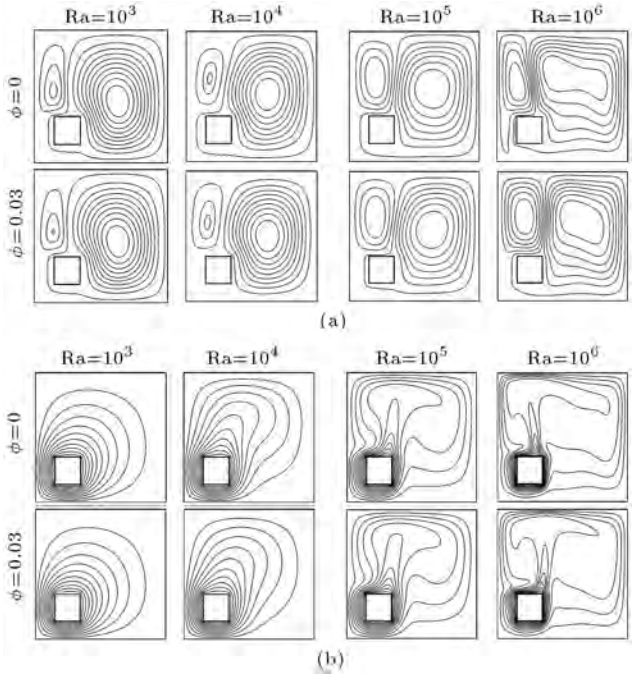

Figure 6. Streamlines and isotherms in the cavity filled with TiO_2-water for case III: (a) Streamlines; and (b) isotherms.

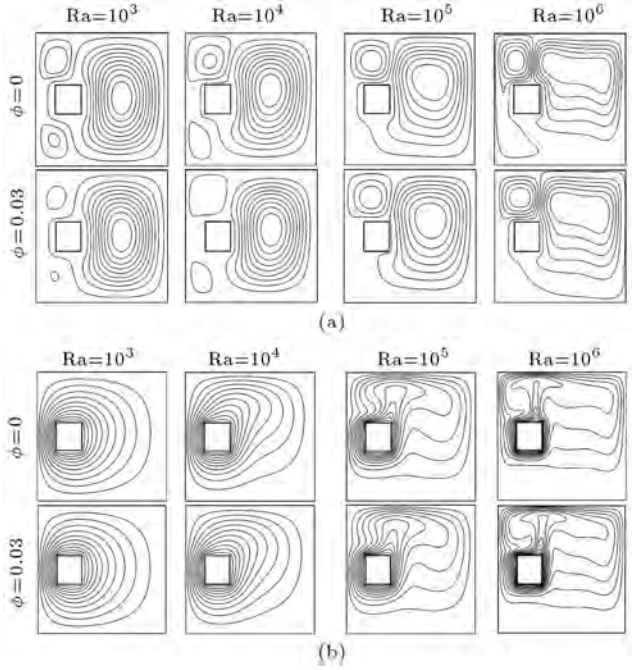

Figure 7. Streamlines and isotherms in the cavity filled with TiO_2-water for case IV: (a) Streamlines; and (b) isotherms.

(b), respectively. Similar to the previous case, a main clockwise vortex develops to the right of the heat source, in this case. For low Rayleigh numbers, this vortex is symmetric, with respect to the horizontal centerline of the cavity (Figure 7(a) for Ra = 10^3). Two smaller eddies also form above and under the

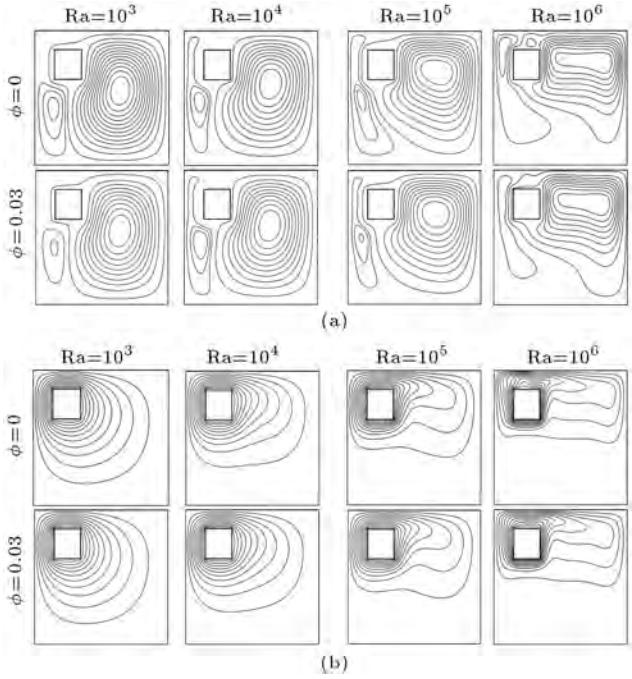

Figure 8. Streamlines and isotherms in the cavity filled with TiO_2-water for case V: (a) Streamlines; and (b) isotherms.

heat source in this case. As the natural convection strengthens with increasing the Rayleigh number, the center of the main eddy shifts toward the top wall of the cavity (Figure 7(a) for Ra = 10^6). Besides, the fluid flow in the top small eddy intensifies, while the eddy under the heat source vanishes as a result of the heat source resisting the natural convection close to the bottom left corner of the cavity (Figure 7(a) for Ra = 10^6). Moreover, the former eddy shrinks as the volume fraction of the nanoparticles and, in turn, the nanofluid viscosity increase. As far as the isotherms are concerned, the highest temperature gradient occurs in the boundary layer close to the top wall of the cavity above the heat source for Ra = 10^6. Furthermore, for high Rayleigh numbers, the heat transfer rate in the stagnant region above the bottom wall of the cavity is negligible (Figure 7(b) for Ra $\geq 10^5$).

Figure 8(a) and (b) show the streamlines and the isotherms inside the cavity for case V. Similar to the previous case, here, a main clockwise vortex develops to the right of the heat source due to natural convection. Also, a smaller counterclockwise eddy forms in the left lower portion of the cavity (Figure 8(a)). As the natural convection strengthens, the centers of these eddies shift toward the top wall of the cavity, consequently, a relatively stagnant and isothermal region with negligible heat transfer rate emerges in the bottom of the cavity (Figure 8(a) and (b) for Ra = 10^6). Moreover, the counterclockwise eddy weakens as the Rayleigh number increases and, even more eminently, as both the Rayleigh number and the volume fraction of

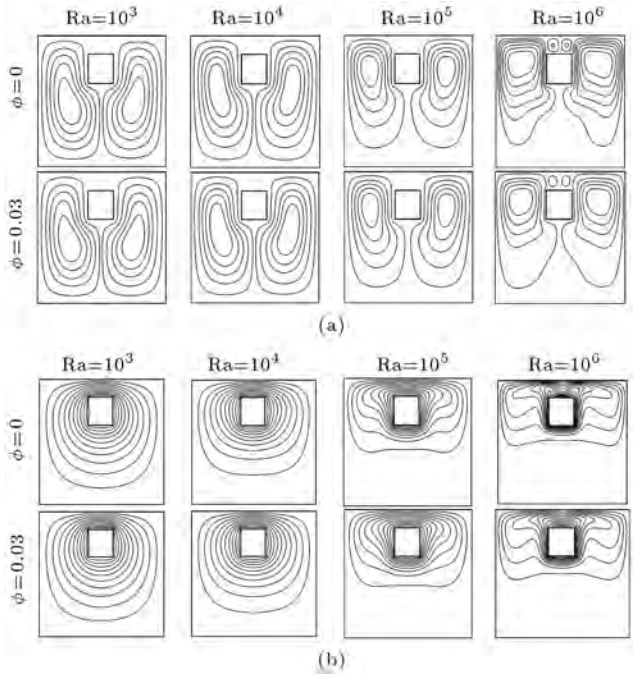

Figure 9. Streamlines and isotherms in the cavity filled with TiO_2-water for case VI: (a) Streamlines; and (b) isotherms.

the nanoparticles increase. For low Rayleigh numbers, the isotherms are concentrated in the narrow spaces above and to the left of the heat source, resulting in high heat transfer rates there (Figure 8(b) for $Ra \geq 10^4$). As the Rayleigh number increases, thermal boundary layers with high temperature gradients and relatively large heat transfer rates develop along the cavity's top wall above the heat source (Figure 8(b) for $Ra \geq 10^5$).

The streamlines and the isotherms for case VI are shown in Figure 9(a) and (b), respectively. Similar to case I, two counter-rotating vortices are present inside the cavity in this case. However, two smaller counter-rotating eddies, similar to the Bernard cells, develop in the gap between the top walls of the heat source and the cavity for $Ra = 10^6$, in this case (Figure 9(a)). These latter eddies contract as the volume fraction of the nanoparticles and, in turn, the effective viscosity of the nanofluid increase. As far as the isotherms are concerned, for low Rayleigh numbers, high temperature gradients are observed in the gap above the heat source (Figure 9(b) for $Ra \leq 10^4$). For the convection-dominated heat transfer regime, thermal boundary layers develop along the cavity's top wall, resulting in a high rate of heat transfer there, while the lower portion of the cavity is nearly isothermal with negligible heat transfer (Figure 9(b) for $Ra \geq 10^5$).

Figure 10 shows the Nusselt number distributions along the walls of the cavity for the six considered cases. The results are presented for $Ra = 10^3$ and for three different volume fractions of the nanoparticles, namely, 0.0 (pure fluid), 0.015 and 0.03. For $Ra = 10^3$, the heat transfer occurs mainly through conduction. It is seen from this figure that, for case I, where the heat source is placed at the middle of the cavity, each cavity wall has nearly the same Nusselt number distribution with a local maximum at its middle. As the volume fraction of the nanoparticles and, in turn, the thermal conductivity of the nanofluid increase, the Nusselt number rises, implying enhanced heat transfer. For the other cases shown in this figure, the maximum local Nusselt number occurs along the walls having minimum distance from the heat source, while the Nusselt number is quite low along the remaining walls. Moreover, the local maxima of Nusselt number for cases II through VI are significantly higher than those of case I. Increasing the volume fraction of the nanoparticles for cases II through VI increases the local maxima of the Nusselt number significantly (Figure 10).

The Nusselt number distributions along the cavity walls for $Ra = 10^6$ and for the six considered cases are presented in Figure 11. The results in this figure are for three different volume fractions of the nanoparticles, namely, 0.0, 0.015 and 0.03. As seen from this figure, for case I, contrary to the results of Figure 10, the maximum local Nusselt number occurs at the middle of the cavity's top wall, while the Nusselt number is quite low along its bottom wall. Moreover, the heat transfer enhancement, with increasing the volume fraction of the nanoparticles, is marginal in this convection-dominated heat transfer regime, as a result of the nanofluid becoming more viscous, by raising the nanoparticles volume fraction. For case II, similar to the previous case, the local Nusselt number has a maximum at the middle of the cavity's top wall, whose magnitude, nevertheless, is smaller compared to that of case I, due to the eddies being weaker in the latter case. For cases II through V, the maximum local Nusselt number occurs in the thermal boundary layers towards the left portion of the top wall of the cavity, where the temperature gradient is relatively high (Figure 11). Moreover, the highest local Nusselt number among these cases belongs to case V, for which the heat source has the smallest distance from the cavity's top wall. For case VI, the Nusselt number has two local maxima along the top wall of the cavity, which are symmetrically-located, with respect to the cavity's vertical centerline, with the Nusselt number decreasing substantially between them (Figure 11). This particular distribution of Nusselt number is attributed to the formation of two small eddies above the top wall of the heat source, in this case (Figure 9(a)).

Figure 12 shows the variations of the average Nusselt number of the cavity for the six con-

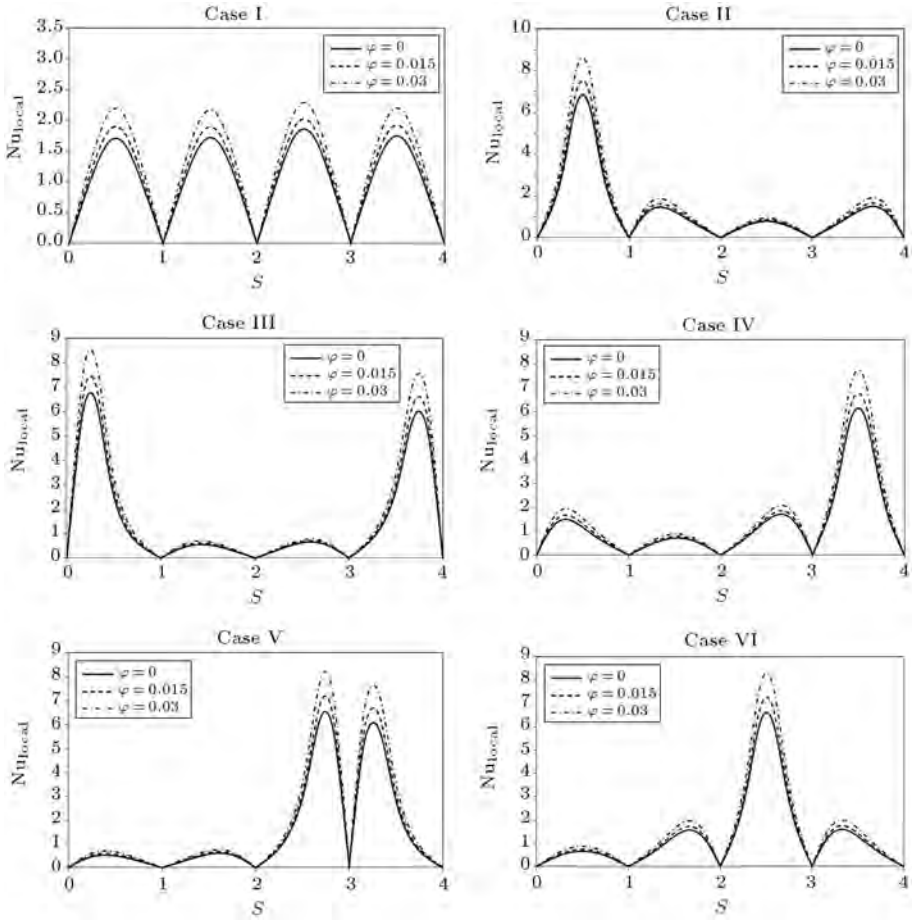

Figure 10. local Nusselt number along the cold walls of the cavity for the six different locations of the heat source, $Ra = 10^3$, and $\varphi = 0.0$, 0.015, and 0.03.

sidered cases, with respect to the volume fraction of the nanoparticles for different Rayleigh numbers.

It is observed from the figure that for conduction-dominated heat transfer regime, $Ra = 10^3$, the average Nusselt number for all the considered cases significantly increases with increasing the volume fraction of the nanoparticles, a characteristic which is attributed to the thermal conductivity enhancement by increasing the volume fraction of the nanoparticles. Moreover, as the geometry and the boundary conditions for cases III and V are alike, as far as conduction heat transfer is concerned, their average Nusselt numbers should be the same for the entire range of the considered volume fraction of the nanoparticles (Figure 12 for $Ra = 10^3$). By the same token, cases II, IV, and VI ought to have similar average Nusselt number, as demonstrated in Figure 12, for $Ra = 10^3$. The maximum heat transfer rate belongs to either of cases III or V, where the heat source is located close to two of the cavity walls, while the minimum heat transfer rate pertains to case I, with the heat source at the center of the cavity (Figure 12 for $Ra = 10^3$).

With increasing the Rayleigh number, the average Nusselt number for case V reduces drastically, compared to that of case III, due to significant blockage effects in the narrow gaps between the heat source and the top and left walls of the cavity for the former case (Figure 12 for $Ra \geq 10^4$). In fact, the minimum average Nusselt number for $Ra = 10^6$ pertains to case V. As far as cases II, IV, and VI are concerned, the average Nusselt number for case II increases moderately, compared to that of case IV, with increasing the Rayleigh number. However, for case VI, due to the substantial blockage effect in the narrow gap between the top walls of the heat source and cavity, the average Nusselt number decreases significantly, compared to that of case IV, as natural convection becomes dominant (Figure 12 for $Ra \geq 10^6$). The maximum average Nusselt number for the convection-dominated heat transfer regime pertains to case II, with a minor blockage effect (Figure 12 for $Ra = 10^6$). Moreover, in general, for $Ra \geq 10^4$, the average Nusselt number increases with increasing the volume fraction of the nanoparticles for all the cases, albeit with lower rates, compared to those for $Ra = 10^4$, due to the dominant role played by the viscosity of the nanofluid in high Rayleigh number flows.

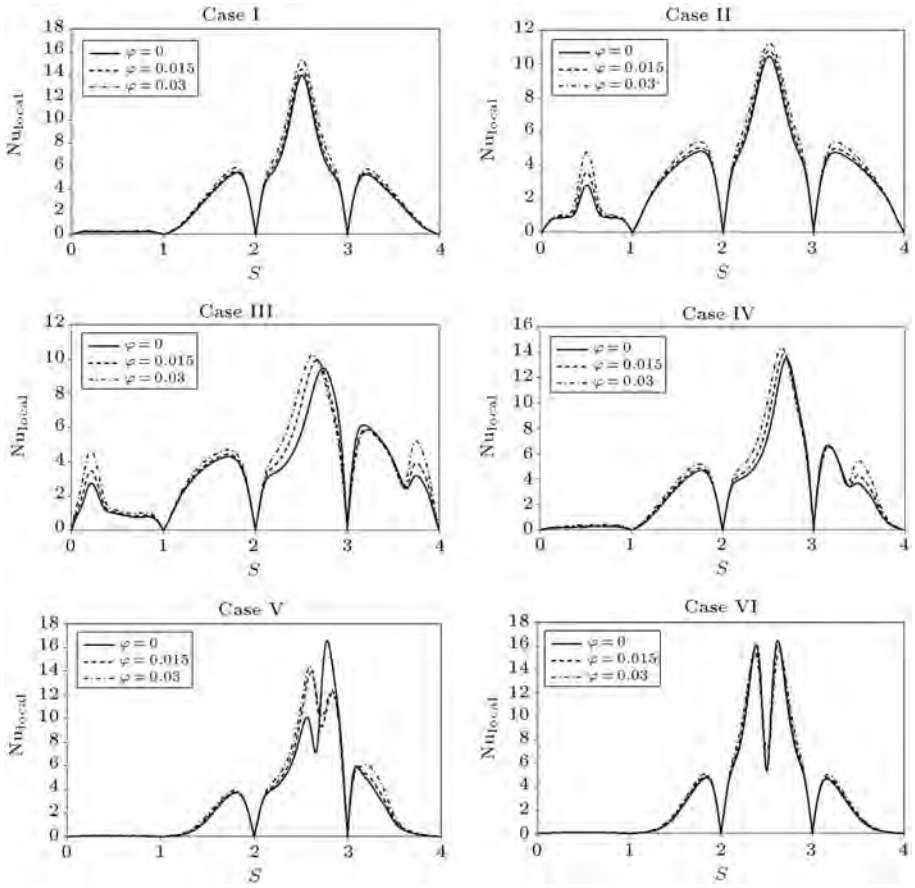

Figure 11. local Nusselt number along the cold walls of the cavity for the six different locations of the heat source, $Ra = 10^6$, and $\varphi = 0.0$, 0.015, and 0.0.

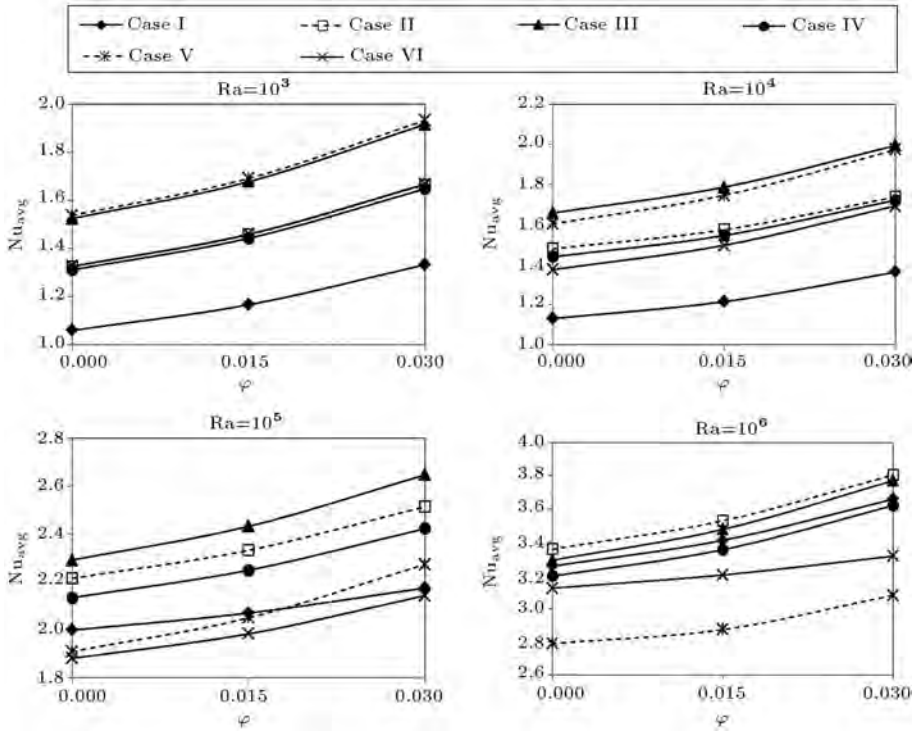

Figure 12. Variations of the average Nusselt number of the cavity with respect to the volume fraction of the nanoparticles for different Rayleigh numbers.

5. Conclusions

Buoyancy-driven fluid flow and heat transfer of TiO_2-water nanofluid, due to the square-shaped heat source inside the square cavity, are simulated numerically. The finite volume method, together with the SIMPLER algorithm, is implemented to solve the governing equations written in terms of the primitive variables. The numerical procedure is verified via simulating the natural convection in a partially-heated square cavity filled with Cu-water nanofluid.

The effects of the location of the heat source inside the cavity, the Rayleigh number, and the TiO_2 volume fraction, on the fluid flow and heat transform are investigated by conducting a parametric study. As far as the position of the heat source inside the cavity is concerned, six different cases, I through VI, are considered. The results, in general, show that the heat source location is eminently an effective parameter controlling the shape and size of eddies formed inside the cavity and, subsequently, the heat transfer rate. For the conduction-dominated heat transfer regime, $Ra = 10^3$, the maximum heat transfer rate is achieved, irrespective of the volume fraction of the nanoparticles, by placing the heat source close to the cavity corners (cases III and V), while the lowest rate heat transfer pertains to case I with the heat source at the center of the cavity. For convection-dominated heat transfer regime, $Ra = 10^6$, the highest rate of heat transfer is accomplished by placing the heat source near the corner of the cavity's bottom wall for the considered range of the volume fraction of the nanoparticles (case II). On the other hand, for the same Rayleigh number, case V, with the heat source positioned towards the top left corner of the cavity, has the lowest Nusselt number, irrespective of the volume fraction of the nanoparticles.

Finally, the results for the local and average Nusselt numbers demonstrate that natural convection heat transfer is much improved in the presence of TiO_2 nanoparticles.

Nomenclature

c_p	Heat capacity
d	Diameter, m
g	Gravitational acceleration, m/s^2
h	Heat source height, m
H	Cavity height, m
k	Thermal conductivity, W/m-K
M	Molecular weight
N	Avogadro number
Nu	Nusselt number
p	Pressure, kg/m-s^2
P	Dimensionless pressure
Pr	Prandtl number
Ra	Rayleigh number
Re	Reynolds number
s	Special coordinate system, m
S	Dimensionless special coordinate system
T	Temperature, K
u, v	Velocity components, m/s
U, V	Dimensionless velocity components
xy	Cartesian coordinates, m
X, Y	Dimensionless Cartesian coordinates

Greek letters

α	Thermal diffusivity, m^2/s
β	Thermal expansion coefficient, 1/K
μ	Viscosity, kg/m-s
v	Kinematics viscosity, m^2/s
θ	Dimensionless temperature
ρ	Density, kg/m^3
φ	Volume fraction of nanoparticles

Subscript

avg	Average
c	Cold
f	Fluid
h	Hot
nf	Nanofluid
p	Particle

References

1. Khanafer, K., Vafai, K. and Lightstone, M. "Buoyancy-driven heat transfer enhancement in a two-dimensional enclosure utilizing nanofluid", *Int. J. Heat Mass Transf.*, **46**, pp. 3639-3653 (2003).

2. Abu-Nada, E., Masoud, Z. and Hijazi, A. "Natural convection heat transfer enhancement in horizontal concentric annuli using nanofluids", *Int. Comm. Heat Mass Transf.*, **35**, pp. 657-665 (2008).

3. Santra, A.K., Sen, S. and Chakraborty, N. "Study of heat transfer augmentation in a differentially heated square cavity using copper-water nanofluid", *Int. J. Therm. Sci.*, **47**, pp. 1113-1122 (2008).

4. Oztop, H.F. and Abu-Nada, E. "Numerical study of natural convection in partially heated rectangular enclosures filled with nanofluids", *Int. J. Heat Fluid Flow*, **29**, pp. 1326-1336 (2008).

5. Abu-nada, E. and Oztop, H. "Effect of inclination angle on natural convection in enclosures filled with

Cu-water nanofluid", *Int. J. Heat Fluid Flow*, **30**, pp. 669-678 (2009).

6. Aminossadati, S.M. and Ghasemi, B. "Natural convection cooling of a localized heat source at the bottom of a nanofluid-filled enclosure", *Eur. J. Mech. B/Fluids*, **28**, pp. 630-640 (2009).

7. Ghasemi, B. and Aminossadati, S.M. "Periodic natural convection in a nanofluid-filled enclosure with oscillating heat flux", *Int. J. Therm. Sci.*, **49**, pp. 1-9 (2010).

8. Oztop, H.F., Abu-Nada, E., Varol, Y. and Al-Salem, K. "Computational analysis of non-isothermal temperature distribution on natural convection in nanofluid filled enclosures", *Superlattic. Microstruct.*, **49**, pp. 453-467 (2011).

9. Sheikhzadeh, G.A., Arefmanesh, A. and Mahmoodi, M. "Numerical study of natural convection in a differentially-heated rectangular cavity filled with TiO_2-water nanofluid", *J. Nano Res.*, **13,** pp. 75-80 (2011).

10. Alloui, Z., Vasseur, P. and Reggio, M. "Natural convection of nanofluids in a shallow cavity heated from below", *International Journal of Thermal Sciences*, **50**, pp. 385-393 (2011).

11. Aminossadati, S.M. and Ghasemi, B. "Natural convection of water-CuO nanofluid in a cavity with two pairs of heat source-sink", *International Communications in Heat and Mass Transfer*, **38**, pp. 672-678 (2011).

12. Nasrin, R. and Parvin, S. "Investigation of buoyancy-driven flow and heat transfer in a trapezoidal cavity filled with water-Cu nanofluid", *International Communications in Heat and Mass Transfer*, **39**, pp. 270-274 (2012).

13. Nikfar, M. and Mahmoodi, M. "Meshless local Petrov-Galerkin analysis of free convection of nanofluid in a cavity with wavy side walls", *Engineering Analysis with Boundary Elements*, **36**, pp. 433-445 (2012).

14. Mahmoudi, A.H., Shahi, M., Honarbakhsh Raouf, A. and Ghasemian, A. "Numerical study of natural convection cooling of horizontal heat source mounted in a square cavity filled with nanofluid", *International Communications in Heat and Mass Transfer*, **37**, pp. 1135-1141 (2010).

15. Mahmoudi, A.H., Shahi, M., Moheb Shahedin, A. and Hemati, N. "Numerical modeling of natural convection in an open cavity with two vertical thin heat sources subjected to a nanofluid", *International Communications in Heat and Mass Transfer*, **38**, pp. 110-118 (2011).

16. Cho, C., Yau, H. and Chen, Ch. "Enhancement of natural convection heat transfer in a U-shaped cavity filled with Al_2O_3-water nanofluid", *Thermal Science*, **16**, pp. 1317-1323 (2012).

17. Mahmoodi, M. "Numerical simulation of free convection of a nanofluid in L-shaped cavities", *International Journal of Thermal Sciences*, **50**, pp. 1731-1740 (2011).

18. Mahmoodi, M. and Hashemi, S.M. "Numerical study of natural convection of a nanofluid in C-shaped enclosures", *International Journal of Thermal Sciences*, **55**, pp. 76-89 (2012).

19. Dehnavi, R. and Rezvani, A. "Numerical investigation of natural convection heat transfer of nanofluids in a Γ shaped cavity", *Superlattices and Microstructures*, **52**, pp. 312-325 (2012).

20. Mahmoodi, M. "Numerical simulation of free convection of nanofluid in a square cavity with an inside heater", *International Journal of Thermal Sciences*, **50**, pp. 2161-2175 (2011).

21. Shahi, M., Mahmoudi, A.H. and Talebi, F. "Entropy generation due to natural convection cooling of a horizontal heat source mounted inside a square cavity filled with nanofluid", *Heat Transfer Research*, **43**, pp. 19-46 (2012).

22. Sheikhzadeh, G.A., Nikfar, M. and Fattahi, A. "Numerical study of natural convection and entropy generation of Cu-water nanofluid around an obstacle in a cavity", *Journal of Mechanical Science and Technology*, **26**, pp. 3347-3356 (2012).

23. Mahmoodi, M. and Mazrouei Sebdani, S. "Natural convection in a square cavity containing a nanofluid and an adiabatic square block at the center", *Superlattices and Microstructures*, **52**, pp. 261-275 (2012).

24. Aminossadati, S.M. and Ghasemi, B. "Conjugate natural convection in an inclined nanofluid-filled enclosure", *International Journal of Numerical Methods for Heat & Fluid Flow*, **22**, pp. 403-423 (2012).

25. Arefmanesh, A., Amini, M., Mahmoodi, M. and Najafi, M. "Buoyancy-driven heat transfer analysis in two-square duct annuli filled with a nanofluid", *European J. of Mechanics - B/Fluids*, **33**, pp. 95-104 (2012).

26. Habibi Matin, M. and Pop, I. "Natural convection flow and heat transfer in an eccentric annulus filled by Copper nanofluid", *International Journal of Heat and Mass Transfer*, **61**, pp. 353-364 (2013).

27. Bejan, A. *Convection Heat Transfer*, John Wiley & Sons, Inc., Hoboken, New Jersey, USA (2004).

28. Corcione, M. "Empirical correlating equations for predicting the effective thermal conductivity and dynamic viscosity of nanofluids", *Energy Conversion and Management*, **52**, pp. 789-793 (2011).

29. Patankar, S.V. *Numerical Heat Transfer and Fluid Flow*, Hemisphere Publishing Corporation, Taylor and Francis Group, New York (1980).

Biographies

Ali Arefmanesh received his BS degree from Sharif University of Technology, Tehran, Iran, in 1980, and

MS and PhD degrees in 1987 and 1992, respectively, from the University of Delaware, Newark, USA. He is currently Associate Professor in the Department of Mechanical Engineering at The University of Kashan, Iran. His current research interests are computational fluid dynamics, numerical simulation of fluid flow and heat transfer of nanofluids, and meshless numerical methods.

Mostafa Mahmoodi received his BS degree in Mechanical Engineering (Thermo Fluids) from Yazd University, Yazd, Iran, in 2007, his MS degree in Mechanical Engineering (Energy Conversion) from the University of Kashan, Iran, in 2011, and is currently a PhD degree candidate in Mechanical Engineering at Amirkabir University of Technology, Tehran, Iran. His main areas of research are flow around cubic buildings and natural convection flow simulation.

Mehdi Nikfar received his MS degree from Kashan University, Iran, in 2009, and is currently working towards his PhD degree in K.N. Toosi University of Technology, Tehran, Iran. His main research interests are numerical simulation of natural convection flow, meshless methods and CFD.